



# Bevacizumab induces oxidative cytotoxicity and apoptosis via TRPM2 channel activation in retinal pigment epithelial cells: Protective role of glutathione

Dilek Özkaya<sup>1</sup> · Mustafa Nazıroğlu<sup>2,3,4</sup>

Received: 29 September 2020 / Revised: 15 December 2020 / Accepted: 5 January 2021 / Published online: 5 February 2021  
© The Author(s), under exclusive licence to Springer-Verlag GmbH, DE part of Springer Nature 2021

## Abstract

**Purpose** Bevacizumab (BEV) is a blocker of circulating VEGF A generation. However, BEV has adverse apoptotic and cytotoxic effects via upregulation of mitochondrial reactive oxygen species (ROS) and TRPM2 activation, and downregulation of cytosolic glutathione (GSH) in neuronal cells. We investigated the possible protective effects of GSH treatment on BEV-induced oxidant and apoptotic adverse actions in the TRPM2 expressing adult retinal pigment epithelial-19 (ARPE-19) and SH-SY5Y neuronal cells.

**Material and methods** The ARPE-19 and SH-SY5Y cells were divided into five main groups: Control, GSH (10 mM for 2 h), BEV (0.25 mg/ml for 24 h), BEV+GSH, and BEV+TRPM2 channel blockers (ACA or 2-APB). In the SH-SY5Y cells, the Ca<sup>2+</sup> analyses (Fluo-3) were performed only, although Fluo-3 and the remaining analyses were performed in the ARPE-19 cells.

**Results** The levels of apoptosis, cell death, mitochondrial ROS, lipid peroxidation, caspase-3, caspase-9, ADP-ribose-induced TRPM2 current density, cytosolic-free Zn<sup>2+</sup>, and Ca<sup>2+</sup> were increased by BEV, although their levels were diminished by the treatments of GSH and TRPM2 blockers. The BEV-induced decreases of cell viability, GSH levels, and glutathione peroxidase activities were increased by the treatment of GSH. BEV-induced increase of TRPM2 expression was decreased by the treatment of GSH, although BEV-induced decrease of VEGF A expression was further decreased by the treatment of GSH.

**Conclusion** Our data confirmed that BEV-induced mitochondrial ROS and apoptosis in the human retinal epithelial cells were modulated by GSH and TRPM2 inhibition. The treatment of GSH may be considered as a therapeutic approach to BEV-induced ARPE-19 cell injury.

**Keywords** Apoptosis · ARPE-19 cells · Bevacizumab · Oxidative stress · SH-SY5Y cells · TRPM2 channel

## Abbreviations

[Ca <sup>2+</sup> ] <sub>c</sub>	Intracellular free Ca <sup>2+</sup> concentration
ADPR	ADP-ribose
ARPE-19	Adult retinal pigment epithelial-19
ARPE-19	Adult retinal pigment epithelial-19
BEV	Bevacizumab
BSO	Buthionine sulfoximine
GPx	Glutathione peroxidase
GSH	Glutathione

MDA	Malondialdehyde
ROS	Reactive oxygen species
TAS	Total antioxidant status
TRP	Transient receptor potential
TRPM2	Transient receptor potential melastatin 2
VEGF	Vascular endothelial growth factor

✉ Mustafa Nazıroğlu  
mustafanaziroglu@sdu.edu.tr

<sup>1</sup> Department of Ophthalmology, Faculty of Medicine, Suleyman Demirel University, Isparta, Turkey

<sup>2</sup> Neuroscience Research Center, Suleyman Demirel University, Isparta, Turkey

<sup>3</sup> Drug Discovery Unit, BSN Health, Analyses, Innovation, Consultancy, Organization, Agriculture, Industry and Trade Limited Company, Göller Bölgesi Teknokenti, Isparta, Turkey

<sup>4</sup> Department of Biophysics, Faculty of Medicine, Suleyman Demirel University, 32260 Isparta, Turkey

### Key Messages

- Bevacizumab via  $\text{Ca}^{2+}$  influx and oxidative stress plays important role in retina cytotoxicity.> Activity of TRPM2 is increased in the ARPE-19 cells by bevacizumab> The channel is inhibited in the cells by glutathione treatment.

## Introduction

The retinal pigment epithelial cell is the main source of vascular endothelial growth factor (VEGF) generation. The VEGF stimulates neovascularization in the retinal pigment epithelial cell [1] because it is a pro-angiogenic factor. The treatment of VEGF induces cellular migration, proliferation, and survival via activation of oxidative signaling pathways and phosphorylation of VEGF receptors [2]. Reactive oxygen species (ROS) have been reported to provoke VEGF A generation via the store of oxidized proteins in Bruch's membrane in patients with several eye diseases [3–5]. The excessive generations of ROS in several metabolic diseases such as diabetes and acute inflammation induce oxidative injury in the lens and retinal pigment epithelial cells [6, 7]. In the metabolic diseases, production of VEGF causes oxidant cytotoxicity and apoptosis adverse effect via activations of VEGF receptors, phosphoinositide 3-kinases, and Akt molecular pathways in the retinal pigment epithelial cells [8–10]. However, interaction between ROS-activated transient receptor potential 2 (TRPM2) channel signaling pathway and BEV has not been clarified yet.

In the last decades, it was reported that intravitreally administration of the new antiangiogenic drugs induced protective actions against neovascularization in the diseases of adults and newborns such as diabetic retinopathy, age-related macular degeneration, and retinopathy of prematurity [8–11]. One of the new antiangiogenic drugs is bevacizumab (BEV). The BEV is used as treatment of angiogenesis via inhibition of VEGF generation in the diseases of adults and newborns [11]. Although BEV is an effective drug in the treatment of angiogenesis, it has also several adverse effects such as apoptosis and inflammation in the adult retinal pigment epithelial-19 (ARPE-19) cells [12, 13]. Recent data indicated that the adverse effect of BEV is induced by upregulation of mitochondrial oxidative stress and downregulation of antioxidants such as glutathione (GSH) and glutathione peroxidase (GPx) [14–16]. The depletion of GSH via the treatment of buthionine sulfoximine (BSO) increases permeabilization in the retinal pigment epithelial cell [17]. Contrary, BEV acted the antioxidant action via supporting the cytosolic GSH level in the GSH depletion (via BSO treatment)-induced retinal ganglion cell [18]. Hence, the protective action of GSH on BEV-

induced mitochondrial oxidative stress, apoptosis, and cell death should be clarified in the ARPE-19 cells.

In addition to the apoptotic and oxidant actions of BEV, it increases the intracellular free  $\text{Ca}^{2+}$  concentration ( $[\text{Ca}^{2+}]_c$ ) via activation of transient receptor potential (TRP) vanilloid 1 activation in human osteoblast-like cell line [19]. A member of the TRP superfamily is TRP melastatin 2 (TRPM2) [20]. TRPM2 is activated in several cells, including ARPE-19 cells by ROS, ADP-ribose (ADPR), and  $\text{NAD}^+$  [21, 22]. In addition, TRPM2 activation via GSH depletion in hippocampus [23, 24], dorsal root ganglion (DRG) [25, 26], and microglia [27, 28] was recently reported. However, the GSH treatment-induced inhibition of apoptosis and mitochondrial ROS via the modulation of TRPM2 channel in the hippocampus [23, 24], DRG [25, 26], microglia [27, 28], and HEK293 cells [29, 30] was also reported. Accumulating evidence indicated that the increase of the excessive  $[\text{Ca}^{2+}]_c$  via activation of TRPM2 results in increase of apoptosis in the ARPE-19 cells [31]. The involvement ROS-dependent TRPM2 activation VEGF-induced angiogenesis and postischemic neovascularization in mice was also reported [32]. Hence, BEV-induced excessive  $[\text{Ca}^{2+}]_c$  via activation of TRPM2 channel in ARPE-19 cells might be modulated by the GSH treatment.

The oxidative cytotoxic effect of BEV might induce apoptosis, cell death, and downregulation of GSH levels via activation of TRPM2 in the ARPE-19 cells. However, the effect may be modulated by the GSH treatment. The subjects have not been fully clarified in the ARPE-19 cells under oxidative stress and TRPM2 activation. Our research, therefore, focused on evaluating the protective effects of GSH against BEV-induced adverse effects such as apoptosis,  $\text{Ca}^{2+}$  influx, TRPM2 current density, cytosolic, and mitochondrial ROS release in the cells and the possible model protective action of GSH against adverse oxidative cytotoxicity effect of intravitreal BEV injections in patients. The ARPE-19 cell line spontaneously differentiated from a primary human retinal pigment epithelium (h-RPE) cell [33]. The original ARPE-19 showed specific properties of the h-RPE such as tight junction formation, microvilli, and the expression of the h-RPE-specific genes. Hence, the ARPE-19 cell line is used as a cell model of the h-RPE in the current study as it was used in previous experiments [4, 12, 19].

## Material and methods

### Cell lines

The ARPE-19 cell line was gifted from Dr. Xinhua Shu (Glasgow Caledonian University, UK) to Professor Mustafa Nazıroğlu. The SH-SY5Y cells were purchased from Atlas Biotechnology Inc. (Ankara, Turkey). The naturel presence of TRPM2 channel in the ARPE-19 cells was reported in the results of previous studies by Western blot analyses [31]. Hence, we used the ARPE-19 cells in the current study. Accumulating evidence indicated the naturel presence of the TRPM2 channel in the SH-SY5Y cells [34, 35]. Hence, the cells were used as positive control in the experiment of Fluo-3 in the current study. The ARPE-19 and SH-SY5Y cells were cultured in a medium consisting of Dulbecco's Modified Eagle's Medium (DMEM) (45%) and Ham's F-12 (45%) nutrient medium mixture as described in previous studies [35, 36]. The medium mixture additionally contained fetal bovine serum (10%) and penicillin/streptomycin (1%). Cells in 25-cm<sup>2</sup> flasks with filter cap were grown in cell culture incubator conditions (humidified and 5% CO<sub>2</sub>/95% air atmosphere) (NB-203QS, Gyeonggi-do, South Korea). After counting the cells in an automatic cell counter (Casy Model TT, Roche, Germany), they were seeded in the flasks of five groups at a density of  $1 \times 10^6$  cells per ml.

### Study groups

The ARPE-19 and SH-SY5Y cells in the flasks were divided into four main groups: Control, GSH, BEV, and BEV+GSH.

*First group:* The cells in the control group were kept in the cell culture conditions (37 °C and 5% CO<sub>2</sub>) without GSH and BEV incubations for 26 h.

*Second group:* The cells in the GSH group were incubated by GSH (10 mM) for 2 h [23, 25, 26, 28].

*Third group:* The cells in BEV groups were incubated with BEV (0.25 mg/ml) (Altuzan, Roche Diagnostic Inc., Istanbul, Turkey) for 24 h [19, 37].

*Fourth group:* In the BEV+GSH groups, the cells were incubated with BEV for 24 h and then they were further incubated with GSH for 2 h. In some experiments, the cells were additionally incubated by TRPM2 channel blockers, ACA (25 μM) or 2-APB (100 μM) for 30 min.

In a LSM800 laser-scanning confocal and Axio Observer.Z1/7 microscope (Zeiss, Oberkochen, Germany) analyses, we split the cells for attachment of 35-mm dishes with bottom glasses (Mattek Corporation, Istanbul, Turkey) for each experiment. In a plate reader (Infinite pro200; Tecan Austria GmbH, Grodig, Austria) and patch-clamp analyses, the cells ( $1 \times 10^6$  cells) were seeded on the flask (25 cm<sup>2</sup>) and patch chamber glass, respectively. The analyses of Fluo-3 images were performed in the ARPE-19 and SH-SY5Y cells. The remaining analyses were performed in the ARPE-19 cells only.

### Analyses of lipid peroxidation, GSH, glutathione peroxidase (GPx), and total antioxidant status (TAS) in the ARPE-19 cells

The GSH levels and GPx activity in the ARPE-19 cells were spectrophotometrically (Cary 60 UV-Vis, Agilent, Izmir, Turkey) analyzed at 412 nm according to the methods of Sedlak and Lindsay [38] and Lawrence and Burk [39], respectively. The data of GSH level and GPx activity was indicated as μg/g protein and IU/g protein, respectively. Lipid peroxidation level such as MDA was measured at 532 nm in the spectrophotometer by using the method of Placer et al. [40]. The data of lipid peroxidation was expressed as μg/g protein. TAS concentration in the tissue samples was detected at 660 nm by using a commercial kit of Mega Tip Inc. (Gaziantep, Turkey) [41]. Results of TAS were expressed as μM of H<sub>2</sub>O<sub>2</sub> equivalent of 10<sup>6</sup> ARPE-19 cells.

### The determination of intracellular free Ca<sup>2+</sup> concentration ([Ca<sup>2+</sup>]<sub>i</sub>) via Fluo-3 fluorescent stain in the SH-SY5Y and ARPE-19 cells

We assayed BEV-induced changes of [Ca<sup>2+</sup>]<sub>i</sub> via imaging fluorescence (Fluo-3) intensity in the SH-SY5Y and ARPE-19 cells by using the LSM 800 confocal microscope previously described [35, 36]. For the assay, the cells were incubated with 1 μM Fluo-3 AM (Calbiochem GmbH, Darmstadt, Germany) at dark for 60 min. The Fluo-3 stain was excited in the LSM 800 confocal microscope by using a 488-nm argon laser. The SH-SY5Y and ARPE-19 cells were treated with TRPM2 channel blocker (2-APB, 100 μM) to inhibit Ca<sup>2+</sup> entry before stimulation of TRPM2 (hydrogen peroxide, H<sub>2</sub>O<sub>2</sub> and 1 mM). The fluorescence intensity of Fluo-3 was analyzed at 515 nm in the cells by the LSM 800 confocal microscope (objective 40 × 1.3 oil). The results of Fluo-3 AM were expressed as arbitrary unit (a.u).

### Electrophysiology in the ARPE-19 cells

Whole cell patch-clamp records were taken in the ARPE-19 cells by using an EPC 10 amplifier equipped with Patchmaster software (HEKA, Lamprecht, Germany). In the records ( $n = 6$ ), the holding potential was kept at −65 mV. In the records, the standard extracellular patch chamber solution was containing (in mM) CaCl<sub>2</sub> (1), MgCl<sub>2</sub> (1), KCl (5), NaCl (145), D-glucose (10), and HEPES (10). For preparation of Na<sup>+</sup>-free extracellular patch chamber solution, we used *N*-methyl-D-glucamine (150 mM and NMDG<sup>+</sup>) instead of NaCl (145 mM) (pH 7.4). The pH levels of extracellular and intracellular solutions were adjusted to 7.4 and 7.2, respectively. The borosilicate glass pipettes of patch-clamp were fabricated in the puller (P-97 model, Sutter Instrument Lab, Ankara, Turkey) and the resistance of pipettes was kept between 3 and 7 MΩ. The intracellular [Ca<sup>2+</sup>]<sub>i</sub> was adjusted to 1 μM instead of

0.1  $\mu\text{M}$  because the TRPM2 is activated in the presence of high intracellular  $[\text{Ca}^{2+}]_i$  [42]. The cells were perfused with the standard intracellular solution, containing ADPR (1 mM in patch pipette) for stimulation or ACA (25  $\mu\text{M}$  in patch chamber) for inhibition. The voltage-clamp electrophysiology current results were expressed as the current density (pA/pF).

### Cell viability assay

The ARPE-19 cells ( $1 \times 10^6$ ) were incubated in the 96-well black plates. The supernatants in the five groups were removed by centrifugation (1000g for 5 min), and the cells were washed 3 times with  $1 \times \text{PBS}$ . MTT (Sigma-Aldrich Inc.) was dissolved as 0.5 mg/ml. After adding MTT (200  $\mu\text{l}$ ) to each well, the plates were incubated for 3 h at 37 °C in the incubator (NB-203QS). Absorbance was recorded at 490 nm using a microplate reader (Infinite pro200). After calculating the optic density/mg protein, the levels of cell viability were expressed as percentage.

### Death/live cell rate analyses

Hoechst 33342 as a fluorescence dye stains DNA of live cells and its image represents blue color in the LSM 800 confocal microscope. Propidium iodide (PI) is only permeant to the dead cells and its image represents red color in the confocal microscope. For identification of the death/live cell rate, the cell was incubated with PI (1  $\mu\text{M}$ ) and Hoechst 33342 (2  $\mu\text{M}$ ) dye combination for 30 min at dark. The PI and Hoechst 33342 were purchased from Cell Signaling Technology (Leiden, The Netherlands). After washing the stains with extracellular buffer with  $\text{Ca}^{2+}$  (1.2 mM), the cells were imaged in the confocal microscope (LSM 800) fitted with a  $20 \times$  objective by using the ZEN software (Zeiss). The rate of death (PI)/live (Hoechst) cell was indicated as percentage.

### Apoptosis, caspase-3, and -9 assays in the ARPE-19 cells

The levels of apoptosis in the ARPE-19 cells were measured at 550 nm in the spectrophotometer (Cary 60 UV-Vis) following the manufacturer's instructions (APOPercentage, Biocolor Ltd. Northern Ireland). Total protein concentration in the cell was measured by using Lowry's method as described in previous studies [6, 23]. After calculating optic density/mg protein, the data were expressed as percentage of control.

As synthetic tetrapeptide fluorogenic substrates, Ac-DEVD-AMC and Ac-LEHD-AFC in ARPE-19 cells are used to identify and quantify the caspase-3 and -9 activities in cells with apoptosis [4, 36]. Hence, we used the Ac-DEVD-AMC- and Ac-LEHD-AFC-specific fluorogenic substrates (Bachem AG, Bubendorf, Switzerland) in the ARPE-19 cells for assaying active caspase-3 and -9. The substrate cleavages of

fluorogenic substrates in the cells were measured with an automatic microplate reader (Infinite pro200) (excitation 360 nm, emission 460 nm). The fluorescence measurements of the Ac-DEVD-AMC and Ac-LEHD-AFC were normalized to total protein concentration. The data were indicated as percentage of control.

### Analyses of cytosolic and mitochondrial ROS generations

The ROS generation of mitochondria (MitoROS) was imaged in the confocal microscope by the incubation of 1  $\mu\text{M}$  fluorescent dye (MitoTracker Red CM-H2Xros, Life Technologies) at 37 °C in the dark for 25 min [28, 35]. Before imaging the cells ( $1 \times 10^6$ ) in the dishes (Mattek Corporation), the dye was removed by washing with  $1 \times \text{PBS}$ . The diode laser excitation wavelength of MitoTracker Red CM-H2Xros was kept at 561 nm. The excitation and emission wavelengths of the MitoROS probe were kept at 576 and 598 nm in the ZEN software, respectively. The mean fluorescence intensity results of DCFH-DA ( $n = 25\text{--}30$ ) were expressed as arbitrary unit (a.u.).

The ARPE-19 cells ( $1 \times 10^6$ ) in the dishes (Mattek Corporation) were labeled by using the 10  $\mu\text{M}$  of 2',7'-dichlorofluorescein diacetate (DCFH-DA) (Invitrogen Inc., Oregon, USA) at 37 °C in the dark for 25 min. DCF is a fluorescence form of DCFH-DA and its intensity was measured with excitation (504 nm) and emission (525 nm) settings. The excitation wavelength of laser in the confocal microscope was kept at 488 nm [28, 35]. Each treatment ( $n = 25\text{--}30$ ) was analyzed by the ZEN software. The mean fluorescence intensity results of DCFH-DA were expressed as arbitrary unit (a.u.).

### The measurement of the mitochondrial membrane depolarization (Mit-Dep) levels in the ARPE-19 cells

For the assay of Mit-Dep, the ARPE-19 cells ( $1 \times 10^6$ ) in the dishes were incubated with 5  $\mu\text{M}$  JC-1 stain (Cayman Inc., Istanbul, Turkey) for 30 min at 37 °C in dark. The ratio of the fluorescent intensity was obtained by the excitation (595 nm) to the fluorescent intensity of the emission (535 nm). The fluorescence intensities of JC-1 ( $n = 25\text{--}30$ ) in the LSM 800 confocal microscope were analyzed by using the ZEN software (Zeiss). The results of mean fluorescence intensity were expressed as arbitrary unit (a.u.).

### The analyses of intracellular free $\text{Zn}^{2+}$ concentration ( $[\text{Zn}^{2+}]_i$ ) in the ARPE-19 cells

The active form of FluoZin-3 with fluorescent green color is produced in cytosol of cells from cell permanent  $\text{Zn}^{2+}$  indicator, RhodZin3-AM, because the FluoZin3 exhibits high  $\text{Zn}^{2+}$ -



binding affinity in the labile  $Zn^{2+}$  pool. After addition of 1  $\mu$ M RhodZin3-AM (Thermo Fisher Scientific), the ARPE-19 cells were incubated at 37 °C in the dark for 30 min. After washing the RhodZin3-AM stain with extracellular buffer, the cells were imaged in the laser confocal microscope with excitation (493 nm) and emission (513 nm) settings. The excitation wavelength of laser was kept at 488 nm (objective: Plan Apochromat 40  $\times$  1.3 oil). Each treatment ( $n = 25$ –30) in a group was assayed by the ZEN software. The mean fluorescence intensity results were expressed as arbitrary unit (a.u.).

### Western blot analysis in the ARPE-19 cells

The Western blot analysis ( $n = 3$ ) was performed by using standard Western blotting methods as described in previous studies [6, 23]. After measuring the protein concentration in the ARPE-19 cells ( $5 \times 10^6$ ) by using Lowry's method, the proteins were separated by using electrophoresis on SDS-PAGE and they were transferred electrophoretically on the nitrocellulose membrane (Thermo Scientific). The membranes were blocked for 45 min in 5% nonfat milk and then were incubated overnight with antibodies against human TRPM2 and VEGF A (Cell Signaling Technology) at 4 °C. For the equal protein loading,  $\beta$ -actin protein bands were used as control. The bands of Western blot were imaged in Gel Imagination System (G:Box, Syngene, UK) by using enhanced chemiluminescence Western horseradish peroxidase substrate (Thermo Fischer Scientific). The band intensities of TRPM2 and VEGF were measured by using ImageJ software. The housekeeping protein,  $\beta$ -actin, served as an internal control. The intensity results of TRPM2 and VEGF A were normalized relative to control values.

### Statistical analysis

Mean  $\pm$  standard deviation (SD) was used for presentation of the data. Presence of statistical significance in the SPSS program was tested by using one-way analysis of variance (ANOVA). The individual comparisons as  $p$  ( $\leq 0.05$ ) values were detected by using Student's  $t$  test.

## Results

### The BEV treatment-induced changes of MDA, GSH, GPx, and TAS levels were attenuated in the ARPE-19 cells by the treatments of GSH and 2-APB

The results of MDA, GSH, GPx, and TAS are shown in Table 1. The GPx activity, GSH concentration, and TAS level were decreased in the ARPE-19 cells by the treatment of BEV, although the levels of MDA were increased in the cells by the BEV treatment ( $p \leq 0.05$ ). However, the GPx activity,

GSH concentration, and TAS level were increased in the ARPE-19 cells by treatments of GSH and 2-APB, whereas MDA levels in the cells were decreased by the treatments ( $p \leq 0.05$ ). The current data indicated GSH, GPx, and TAS lowering effects of BEV in the ARPE-19 cells.

### GSH modulated BEV-induced TRPM2 channel activation in the ARPE-19 cells and SH-SY5Y cells

Involvements of TRP vanilloid 1 (TRPV1), VGCC, and chemical-gated  $Ca^{2+}$  channels on the increase of  $[Ca^{2+}]_c$  in several cells were recently reported [18, 43], although there was no report on the increase of  $[Ca^{2+}]_c$  via TRPM2 activation in the ARPE-19 cells. In addition, accumulating data indicate that GSH acted as TRPM2 modulator role in mice microglia and dorsal root ganglion (DRG) neurons [18, 43]. The natural presence of TRPM2 was confirmed in SH-SY5Y cells by the results of several studies [34, 35]. Hence, we investigated the protective role of GSH on the increase of BEV-induced TRPM2 activation and  $[Ca^{2+}]_c$  in the ARPE-19 and SH-SY5Y cells.

The images of Fluo-3 ( $Ca^{2+}$ ) in the control, GSH, BEV, and BEV+GSH groups in the ARPE-19 cells are shown in Figs. 1a, b, c, and d, respectively. The images  $Ca^{2+}$  in the control, GSH, BEV, and BEV+GSH groups in the SH-SY5Y cells are shown in Figs. 2a, b, c, and d, respectively. The  $[Ca^{2+}]_c$  in BEV groups were significantly ( $p \leq 0.05$ ) increased in the ARPE-19 (Figs. 1e and f) and SH-SY5Y (Figs. 2e and f) cells by  $H_2O_2$  (1 mM) stimulation as compared to the control and GSH groups. However, the  $[Ca^{2+}]_c$  was decreased in the BEV+GSH (Fig. 1e) by the treatment of GSH ( $p \leq 0.05$ ). In addition, the  $[Ca^{2+}]_c$  was decreased in the BEV+2-APB groups by the treatment of 2-APB ( $p \leq 0.05$ ) (Figs. 1f and 2f). Hence, we observed BEV-dependent activation of TRPM2 channels in the ARPE-19 and SH-SY5Y cells.

### Involvement of BEV on the TRPM2 current density in the ARPE-19 cells: protective role of GSH

A TRPM2 activator is ADPR and we observed no current in the absence of intracellular ADPR in the ARPE-19 cells (Fig. 3a). However, the TRPM2 is activated up to 0.75 nA in the Ctr+ADPR group by the ADPR stimulation, although they were returned to control values by the ACA treatments (Fig. 3b). In the BEV groups, ADPR stimulation caused further activation of TRPM2 and we observed high current density (up to 1.15 nA) in the cells (Fig. 3c). The current densities in the BEV groups were returned to control levels by the ACA and NMDG<sup>+</sup> treatments ( $p \leq 0.05$ ) (Fig. 3c). In the BEV+GSH+ADPR (Fig. 3d) and GSH+ADPR (Fig. 3e) groups, we observed no TRPM2 activation via the intracellular ADPR stimulations. The current densities were lower in the

**Table 1** The effects of BEV, GSH, and 2-APB on lipid peroxidation (MDA), reduced glutathione (GSH), total antioxidant status (TAS) levels, and glutathione peroxidase (GPx) activity in the ARPE-19 cells (Mean  $\pm$  SD and  $n = 6$ )

Values	Control	GSH	BEV	BEV+GSH	BEV+2-APB
MDA ( $\mu\text{mol/g}$ protein)	20.80 $\pm$ 2.48	18.90 $\pm$ 3.05	27.80 $\pm$ 2.99*	21.40 $\pm$ 0.99**	22.20 $\pm$ 2.44**
GSH ( $\mu\text{mol/g}$ protein)	11.40 $\pm$ 1.84	13.80 $\pm$ 0.63	8.26 $\pm$ 0.75*	10.70 $\pm$ 0.34**	10.10 $\pm$ 0.22**
GPx (IU/g protein)	21.00 $\pm$ 1.71	24.30 $\pm$ 1.24	15.40 $\pm$ 0.41*	19.70 $\pm$ 0.78**	18.60 $\pm$ 0.65**
TAS ( $\mu\text{mol H}_2\text{O}_2$ Equiv./ $10^6$ cell)	17.40 $\pm$ 0.47	18.10 $\pm$ 2.12	12.00 $\pm$ 0.50*	18.40 $\pm$ 0.49**	23.20 $\pm$ 2.03**

\* $p \leq 0.05$  vs. control and GSH groups\*\* $p \leq 0.05$  vs. BEV group

BEV+ADPR and BEV+GSH+ADPR than in Ctr+ADPR and BEV+ADPR groups ( $p \leq 0.05$ ) (Fig. 3f). These data obviously

evidenced the involvement of BEV on TRPM2 activation in the ARPE-19 cells.

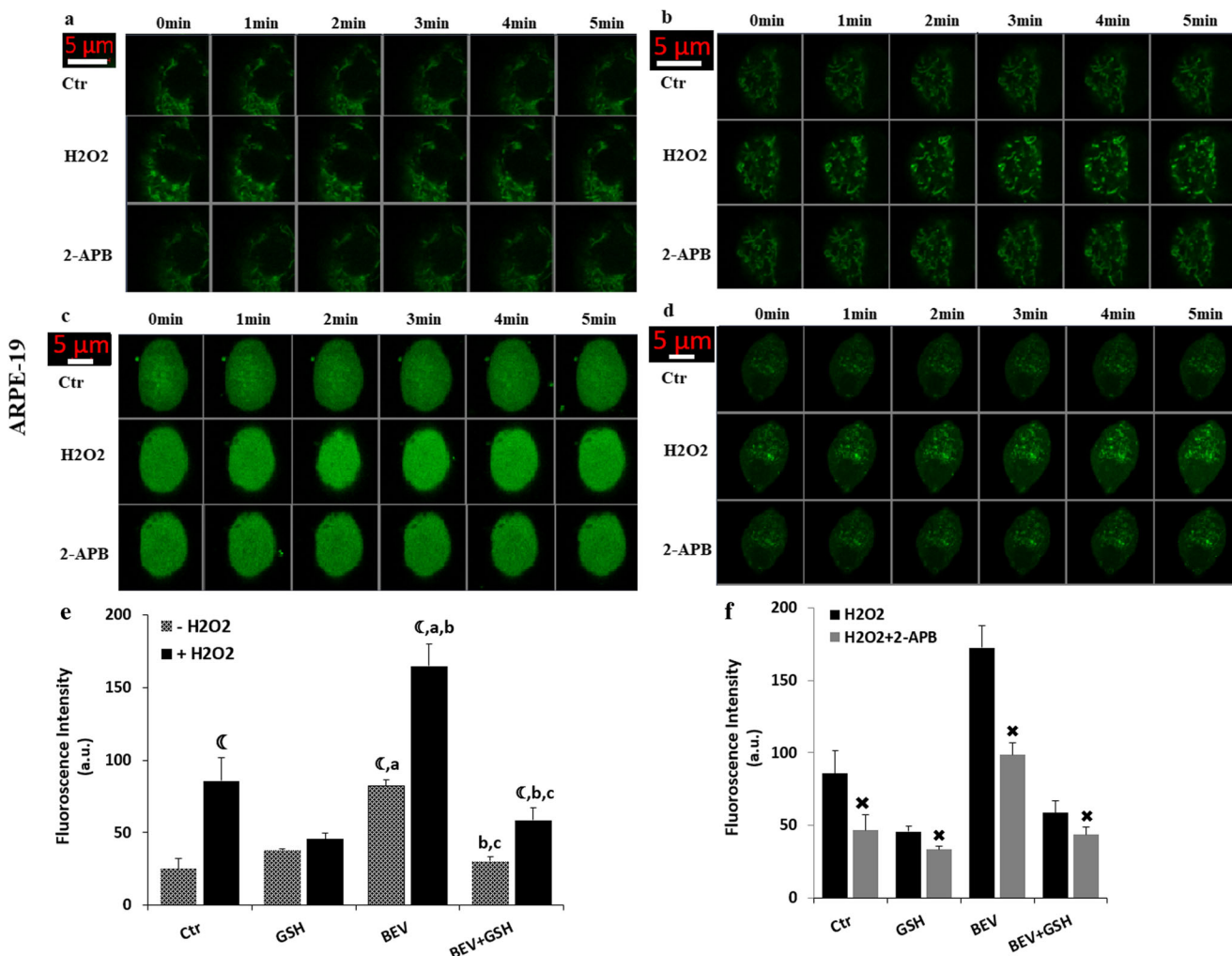


**Fig. 1** The treatment of GSH modulated the BEV-induced increase of Ca<sup>2+</sup> fluorescence intensity via modulation of TRPM2 in the ARPE-19 cells (Mean  $\pm$  SD and  $n = 20$ ). Four groups, control (Ctr), GSH (10 mM for 2 h), BEV (0.25 mg/ml for 24 h), and BEV+GSH, were induced in the ARPE-19 cells. The cells in the four groups were incubated with Fluo-3 (1  $\mu\text{M}$  for 60 min) as a Ca<sup>2+</sup> indicator fluorescent stain. The cells were stimulated with a TRPM2 channel agonist (H<sub>2</sub>O<sub>2</sub>, 1 mM). Then, they were immediately inhibited by the treatment of 2-APB (100  $\mu\text{M}$  for 5 min). The cells were analyzed at 515 nm in the LSM 800 laser scan

microscope (objective 40  $\times$  1.3 oil). The fluorescence intensity of Fluo-3 in the ARPE-19 cells was expressed as arbitrary unit (a.u.). **a**, **b**, **c**, and **d** Images of the Ca<sup>2+</sup> fluorescence intensity in the control (Ctr), GSH, BEV, and BEV+GSH groups respectively. **e** and **f** The changes in the mean Ca<sup>2+</sup> fluorescence intensity in the cells after the treatments of H<sub>2</sub>O<sub>2</sub> and 2-APB treatments, respectively (\* $p \leq 0.05$  vs. absence of H<sub>2</sub>O<sub>2</sub> (-H<sub>2</sub>O<sub>2</sub> group). <sup>#</sup> $p \leq 0.05$  vs. control (Ctr) group. <sup>^</sup> $p \leq 0.05$  vs. GSH group. <sup>~</sup> $p \leq 0.05$  vs. BEV group. <sup>~</sup> $p \leq 0.05$  vs. presence of H<sub>2</sub>O<sub>2</sub> (+H<sub>2</sub>O<sub>2</sub> group)

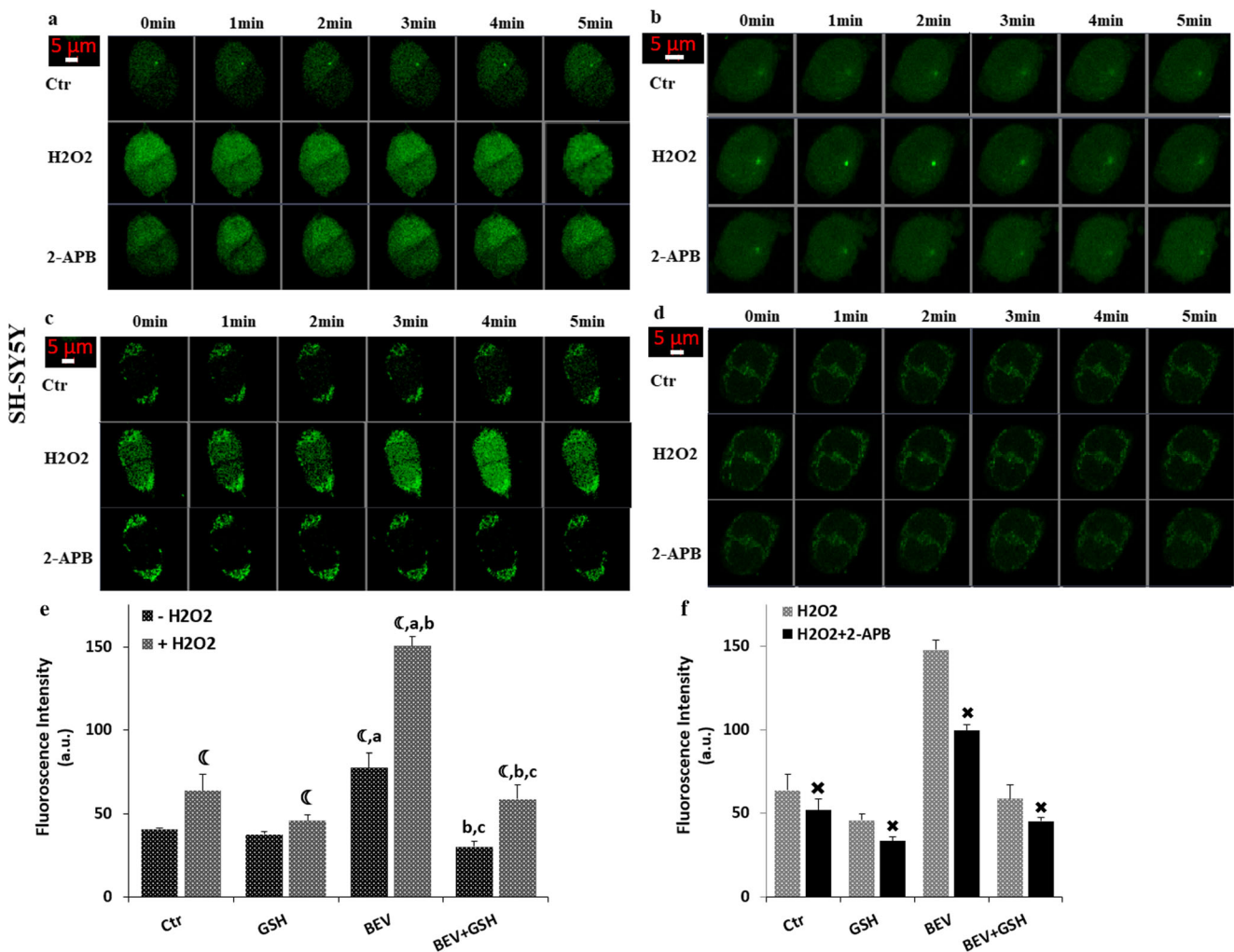


**Fig. 2** The treatment of GSH diminished the BEV-induced increase of Ca<sup>2+</sup> fluorescence intensity via modulation of TRPM2 in the SH-SY5Y cells (Mean  $\pm$  SD and  $n = 20$ ). The four groups, control (Ctr), GSH (10 mM for 2 h), BEV (0.25 mg/ml for 24 h), and BEV+GSH, were induced in the SH-SY5Y cells. The cells in the four groups were incubated with Fluo-3 (1  $\mu$ M for 60 min) as a Ca<sup>2+</sup> indicator fluorescent stain. The cells were stimulated by using a TRPM2 channel agonist (H<sub>2</sub>O<sub>2</sub> and 1 mM). Then, they were immediately inhibited by treatment of 2-APB (100  $\mu$ M for 5 min). The cells were analyzed at 515 nm by the LSC

### The levels of cell viability, apoptosis, caspase-3, and -9 in the ARPE-19 cells were modulated by the treatments of GSH and ACA

Cytosols of cells, including ARPE-19 cells, contain inactive caspases such as caspase-3 and -9 [4, 36, 44]. Apoptosis is induced by the activation of caspase-3 and -9 proteins. Excessive Ca<sup>2+</sup> influx via activation of TRPM2 induces increase of Mit-Dep in several cells [19, 23, 25, 28]. In turn, the increase of Mit-Dep results in the caspase-3 and -9 activations. However, the inhibition of the TRPM2 channel via the treatment of ACA decreases the levels of apoptosis, caspase-3, and -9 in several cells [19, 23, 25, 28]. After observing an increase of [Ca<sup>2+</sup>]<sub>c</sub> and TRPM2 currents in the ARPE-19 cell, we

suspected the increases of apoptosis, caspase-3, and -9, but the decrease of cell viability levels in the cells. The fluorescence intensity of Fluo-3 in the SH-SY5Y cells was expressed as arbitrary unit (a.u.). **a, b, c, and d** Imaging of the Ca<sup>2+</sup> fluorescence intensity in the control (Ctr), GSH, BEV, and BEV+GSH groups respectively. **e and f** Changes in the mean Ca<sup>2+</sup> fluorescence intensity of the cells by H<sub>2</sub>O<sub>2</sub> and 2-APB treatments, respectively (\* $p \leq 0.05$  vs. absence of H<sub>2</sub>O<sub>2</sub> (-H<sub>2</sub>O<sub>2</sub> group). <sup>a</sup> $p \leq 0.05$  vs. control (Ctr) group. <sup>b</sup> $p \leq 0.05$  vs. GSH group. <sup>c</sup> $p \leq 0.05$  vs. BEV group. <sup>c</sup> $p \leq 0.05$  vs. presence of H<sub>2</sub>O<sub>2</sub> (+H<sub>2</sub>O<sub>2</sub> group)

suspected the increases of apoptosis, caspase-3, and -9, but the decrease of cell viability levels in the cells.

The levels of apoptosis (Fig. 4b), caspase-3 (Fig. 4c), and caspase-9 (Fig. 4d) were increased in the BEV groups compared with the control and GSH groups, although cell viability (MTT) level was decreased in the cells by the BEV treatment ( $p \leq 0.05$ ) (Fig. 4a). However, the levels of apoptosis, caspase-3, caspase-9, and cell viability in the ARPE-19 cells were modulated by the treatments of GSH and ACA. The levels of cell viability were decreased in the BEV+GSH and BEV+ACA groups compared to the BEV groups, although apoptosis level, caspase-3, and -9 activities were lower in the BEV+GSH and BEV+ACA groups than in the BEV group ( $p \leq 0.05$ ).

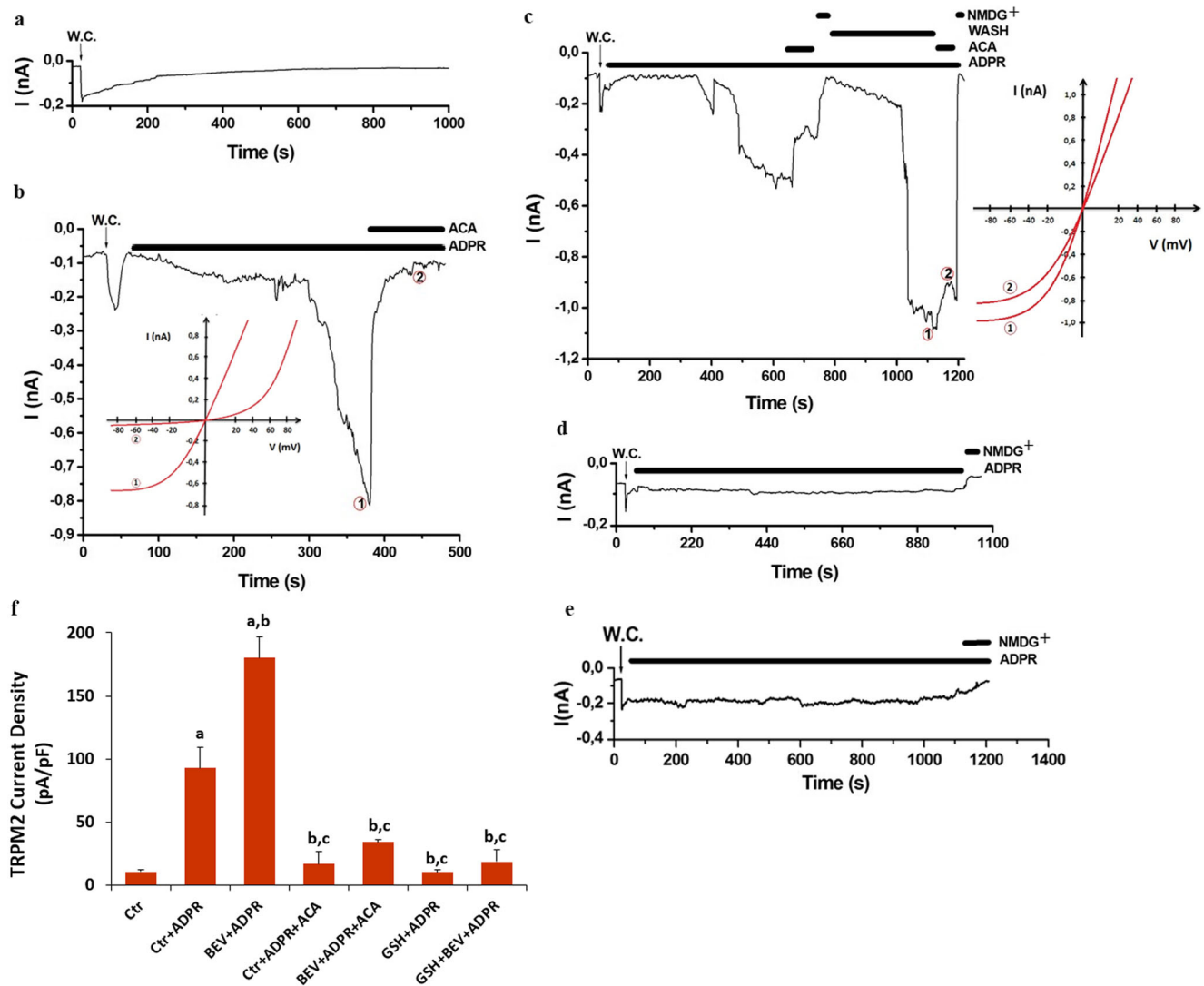


**Fig. 3** Involvement of BEV on the TRPM2 current density in the ARPE-19 cells: Protective role of GSH (Mean  $\pm$  SD and  $n = 6$ ). Whole cell (W.C.) records at  $-65$  mV were taken from the 4 groups. **a** Control (Ctr) group without ADPR stimulation. **b** Ctr+ADPR group. Recordings from TRPM2 inhibited ( $25 \mu\text{M}$  ACA and  $\text{Na}^+$ -free solution-NMDG $^+$ ) in the cells after stimulating intracellular ADPR ( $1 \text{ mM}$  in patch pipette) (without BEV incubation). **c** BEV group. After BEV treatment, the TRPM2 records were taken from the cells by intracellular

ADPR stimulation (with GSH incubation). **d** BEV+GSH group. Recording from ADPR-stimulated cells of BEV+GSH group after BEV and GSH ( $10 \text{ mM}$  for  $2 \text{ h}$ ) treatments. **e** GSH group. Recording from ADPR-stimulated cell of GSH group ( $10 \text{ mM}$  for  $2 \text{ h}$ ) (without BEV incubation). **b** (I–V) and **c** (I–V) are corresponding I/V relation of currents recorded in **b** and **c** at the indicated time points 1 and 2, respectively. **f** Current densities of ARPE-19 cells ( $^a p \leq 0.05$  vs. control (Ctr).  $^b p \leq 0.05$  vs. Ctr+ADPR.  $^c p \leq 0.05$  vs. BEV+ADPR)

BEV-induced cell death (PI/Hoechst) rate in the ARPE-19 cells was decreased by the treatments of GSH and 2-APBs, although cell number was increased by the treatments

The results of recent studies indicate that the depletion of GSH and the increase of ROS generation via activation of TRPM2 induce death of retinal pigment epithelial [31] and neuronal cell [14–16], although GSH treatment modulated the cell death. However, effects of GSH on the BEV-induced apoptosis and cell death in the ARPE-19 cells have not been clarified yet. Hence, we suspected modulator action of GSH against BEV-induced apoptosis and ARPE-19 cell death. We imaged bright field (BF) images in the ARPE-19

cells (Fig. 5a). The images of cell death (Fig. 5b) and 2.5D (Fig. 5c) of the same ARPE-19 cells were recorded in the laser confocal microscope by using ZEN software.

In the present data, the PI/Hoechst cell death rate in the ARPE-19 cells in the BEV group was higher relative to the control and GSH groups ( $p \leq 0.05$ ), although the rate in the cells was significantly ( $p \leq 0.05$ ) higher in the BEV+GSH and BEV+2-APB groups compared to the BEV group (Fig. 5d). However, cell numbers in the ARPE-19 cells were lower in the BEV groups relative to the control and GSH groups ( $p \leq 0.05$ ), although the number in the ARPE-19 cells were significantly ( $p \leq 0.05$ ) higher in the BEV+GSH and BEV+2-APB



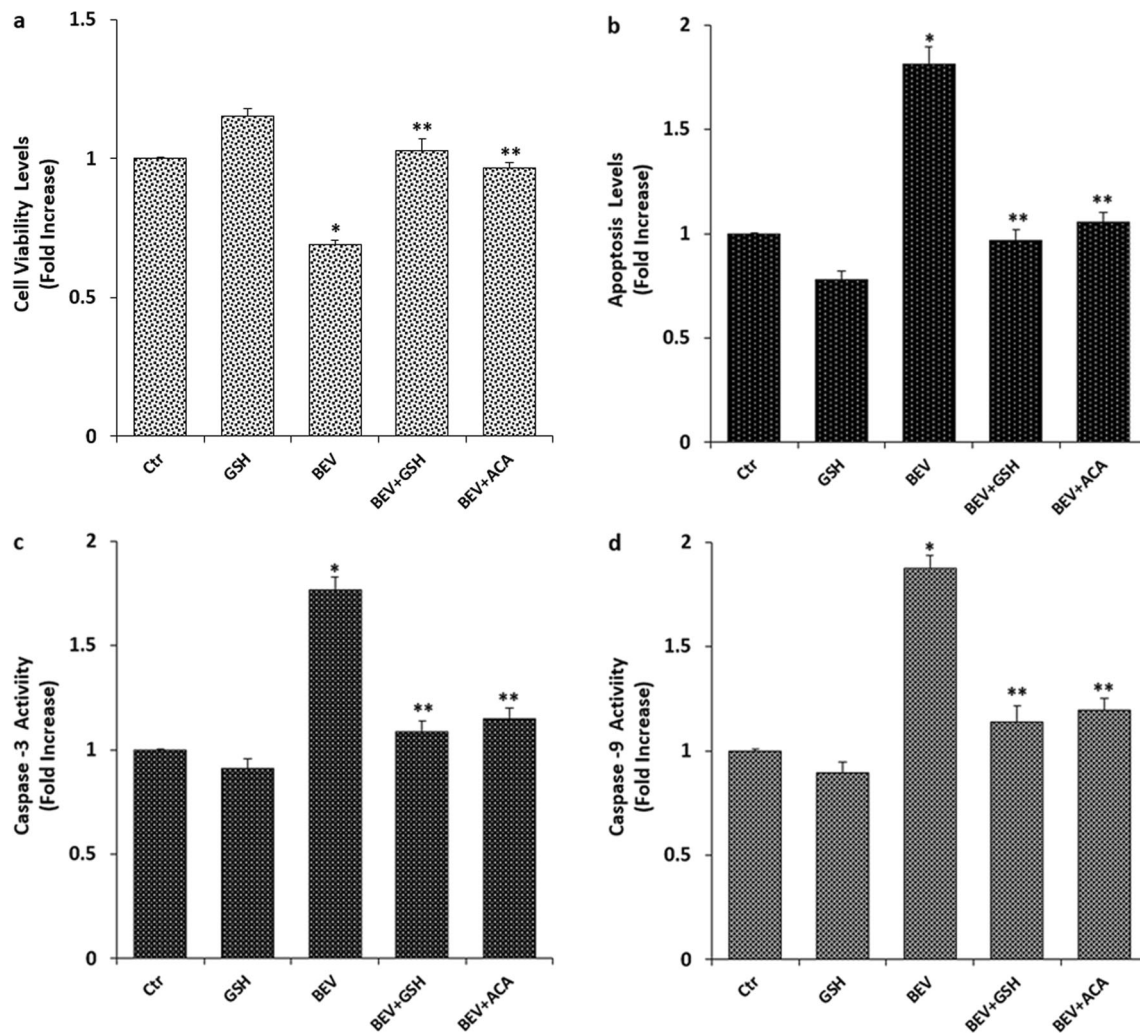


**Fig. 4** The BEV-induced changes of cell viability (MTT), apoptosis, caspase-3, and caspase-9 levels were modulated in the ARPE-19 cells by the GSH and ACA treatments (Mean  $\pm$  SD and  $n = 6$ ). The cells were incubated with GSH (10 mM for 2 h), BEV (0.25 mg/ml for 24 h), and BEV+GSH groups. In the BEV+ACA group, the cells were further

incubated with ACA (25  $\mu$ M) for 30 min after incubations of BEV. Cell viability was analyzed by MTT test (a), whereas apoptosis level (b) was measured by the commercial kit. Caspase-3 and -9 substrates were used for the assays of caspase-3 (c) and caspase-9 (d) (\* $p \leq 0.05$  vs control (Ctr) and GSH groups. \*\* $p \leq 0.05$  vs BEV group)

groups than in the BEV group (Fig. 5e). The data clearly indicated involvement of BEV via activation of TRPM2 in the ARPE-19 cell death. However, the treatment of GSH induced protective action against the increase of ARPE-19 cell death and the decrease of ARPE-19 cell number.

#### **BEV-induced increases of Mit-Dep level, cytosolic (DH123), and mitochondrial ROS (MitoROS) production were modulated in the ARPE-19 cells by the TRPM2 channel blocker (2-APB) and GSH treatments**

The involvement of excessive  $\text{Ca}^{2+}$  influx-dependent ROS via the activation of TRPM2 channel in the induction of apoptosis and death in the several cells except ARPE-19 cells was reported [19, 23, 25, 28]. After observing the increases of cell death and apoptosis levels in the ARPE-19, we suspected

whether DCF, Mit-Dep, and MitoROS generation increased via the increase of TRPM2 activation.

The fluorescence intensities of JC-1 (Figs. 6a and b), DCFH-DA (Figs. 6a and c), and MitoROS (Fig. 6a and d) were increased in the cells with the effect of BEV treatment ( $p \leq 0.05$ ). However, treatments of GSH and 2-APB diminished the effect of BEV via inhibition of  $[\text{Ca}^{2+}]_c$  accumulation, as well as DCFH-DA and MitoROS generations in the ARPE-19 cells ( $p \leq 0.05$ ). The decrease in GSH concentrations following BEV corresponded with increased DCFH-DA and MitoROS generations, although the increases of the DCFH-DA and MitoROS were diminished by the treatments of 2-APB and GSH. Hence, the data of JC-1, DCFH-DA, and MitoROS further supported the effect of GSH on  $[\text{Ca}^{2+}]_c$  and MitoROS-induced ARPE-19 cell death and apoptosis.

## BEV-induced increase of $[Zn^{2+}]_c$ was attenuated in the ARPE-19 cells by the GSH treatment

Accumulation of  $[Zn^{2+}]_c$  induces via depletion of cytosolic GSH increase of Mit-Dep and ROS generation in the lens and retinal cells, although GSH diminished  $[Zn^{2+}]_c$  in the cells [45, 46]. We want to clarify changes of  $[Zn^{2+}]_c$  in the ARPE-19 cells treated with BEV and GSH. The FluoZin3 concentrations were increased in the ARPE-19 cells with the effect of BEV treatment ( $p \leq 0.05$ ). However, GSH treatment diminished the effect of BEV through inhibition of free intracellular  $Zn^{2+}$  accumulation in the cells ( $p \leq 0.05$ ) (Figs. 7a and b).

## The BEV treatment-induced changes of TRPM2 and VEGF expression levels were attenuated in the ARPE-19 cells by the GSH treatment

Accumulating evidences indicate that the increase of TRPM2 expression level causes the increase of  $[Ca^{2+}]_c$  in ARPE-19 and SH-SY5Y cells [31, 35]. It was reported that VEGF expression levels in the ARPE-19 cells were decreased by the BEV treatment [15, 18]. The presence of a direct relationship between VEGF and GSH was also reported in eye cells [11, 17]. However, there is no data on the expression levels of TRPM2 and VEGF in the ARPE-19 cells after the treatment of BEV and GSH. In the current data, the TRPM2 expression level was higher in the BEV group as compared to control and GSH groups ( $p \leq 0.05$ ). However, the treatment of GSH diminished the effect of BEV on the TRPM2 expression levels in the cells and its expression level was lower in the BV+GSH group than in the BEV group ( $p \leq 0.05$ ) (Figs. 8a and b). The BEV-induced decrease of VEGF expression levels was further decreased in the ARPE-19 cells by GSH treatment ( $p \leq 0.05$ ) (Figs. 8a and c).

## Discussion

The GSH is a member thiol redox system, because it has a strong cytosolic antioxidant role in mammalian cells. Hence, the concentration of cytosolic GSH has a major role in the homeostasis of ARPE-19 cells [17]. Several eye diseases such as age-related macular degeneration and diabetes-induced retinal cell injury are induced in ARPE-19 cells by several factors such as the generation of ROS and the depletion of cytosolic GSH [3, 17]. BEV is an effective blocker of VEGF generation in the eye diseases, but it has adverse side effects such as apoptosis and oxidative injury in the ARPE-19 cells [12, 13]. One of the possible reasons in the BEV-induced retinal epithelial cell injury is GSH depletion [11]. Activation of TRPM2 results in apoptosis and oxidative stress in the ARPE-19 [31], SH-SY5Y [35], and neuronal cells [29]. The BEV-induced TRPM2 activation, oxidative stress, and

apoptosis might modulate in the ARPE-19 cells by the GSH treatment. However, the effect of GSH treatment on the BEV-induced apoptosis, death, and mitochondrial oxidative stress generations through TRPM2 activation in the ARPE-19 cells has not yet been clarified. The present data indicate that the modulation of TRPM2 channel in the ARPE-19 and SH-SY5Y cells may serve as an antioxidant redox signaling and apoptosis pathways to mediate the side effects of BEV. Indeed, the data indicated that BEV increased MDA, apoptosis, ARPE-19 cell death, and mitochondrial ROS generation via activation of TRPM2 in the ARPE-19 cells. However, GSH and TRPM2 inhibitors (ACA and 2-APB) reduced the levels of MDA, apoptosis, and ROS in the ARPE-19 cells. Taken together, these results suggest that the treatment of GSH via inhibition overload  $Ca^{2+}$  entry and TRPM2 activation are closely related to the inhibition of BEV-induced cytotoxicity in the ARPE-19 cells.

The activation of TRPM2 in the ARPE-19 and SH-SY5Y cells by oxidative stress and ADPR was recently reported [31, 35]. In addition, GSH depletion induced TRPM2 activation in hippocampus [23, 24], DRG [25, 26], and microglia [27, 28]. However, GSH treatment inhibited TRPM2 in the hippocampus [23, 24], dorsal root ganglion (DRG) [25, 26], microglia [27, 28], and HEK293 cells [29, 30]. To our knowledge, there is no report of GSH on the BEV-induced TRPM2 activation in the ARPE-19 and SH-SY5Y cells. Present Fluo-3 stain and TRPM2 current density data demonstrate that TRPM2 was activated in the ARPE-19 and SH-SY5Y cells by BEV-induced decreases of GSH and GPx. However, GSH treatment inhibited the TRPM2 channel through the inhibition of the ROS generations and the increases of GSH and GPx. The results were confirmed in the ARPE-19 cells by the TRPM2 blockers (ACA and 2-APB). Hence, GSH acted TRPM2 modulator role in the ARPE-19 cells.

The retina is sensitive to the antioxidant balance because of its daily oxygen consumption rate is high. The mitochondria act pivotal functions on the ATP and ROS generation in several cells, including the ARPE-19 cells [4]. BEV has been shown to cause injury to the mitochondria [47]. The BEV-induced decrease of mitochondrial activity via the increase of ROS generation has been reported in rat heart cells and human brain tumors [47, 48]. The GSH depletion and excessive  $Ca^{2+}$  influx-induced Mit-Dep are also involved in the increase of ARPE-19 cell death and decrease of cell viability pathways [47, 48]. Therefore, BEV-induced oxidative stress and TRPM2 activation induce injury in the mitochondria and it may provide a foundation to treat a variety of BEV-caused retinal pigment cell injury. Recently, we demonstrated that the treatment of GSH modulated the levels of apoptosis via the modulation of Mit-Dep and TRPM2 activation in the DRG and hippocampus [23–26]. In the present data, an increase in the Mit-Dep and MDA level was observed in the BEV-treated ARPE-19 cells. However, the level of Mit-Dep was

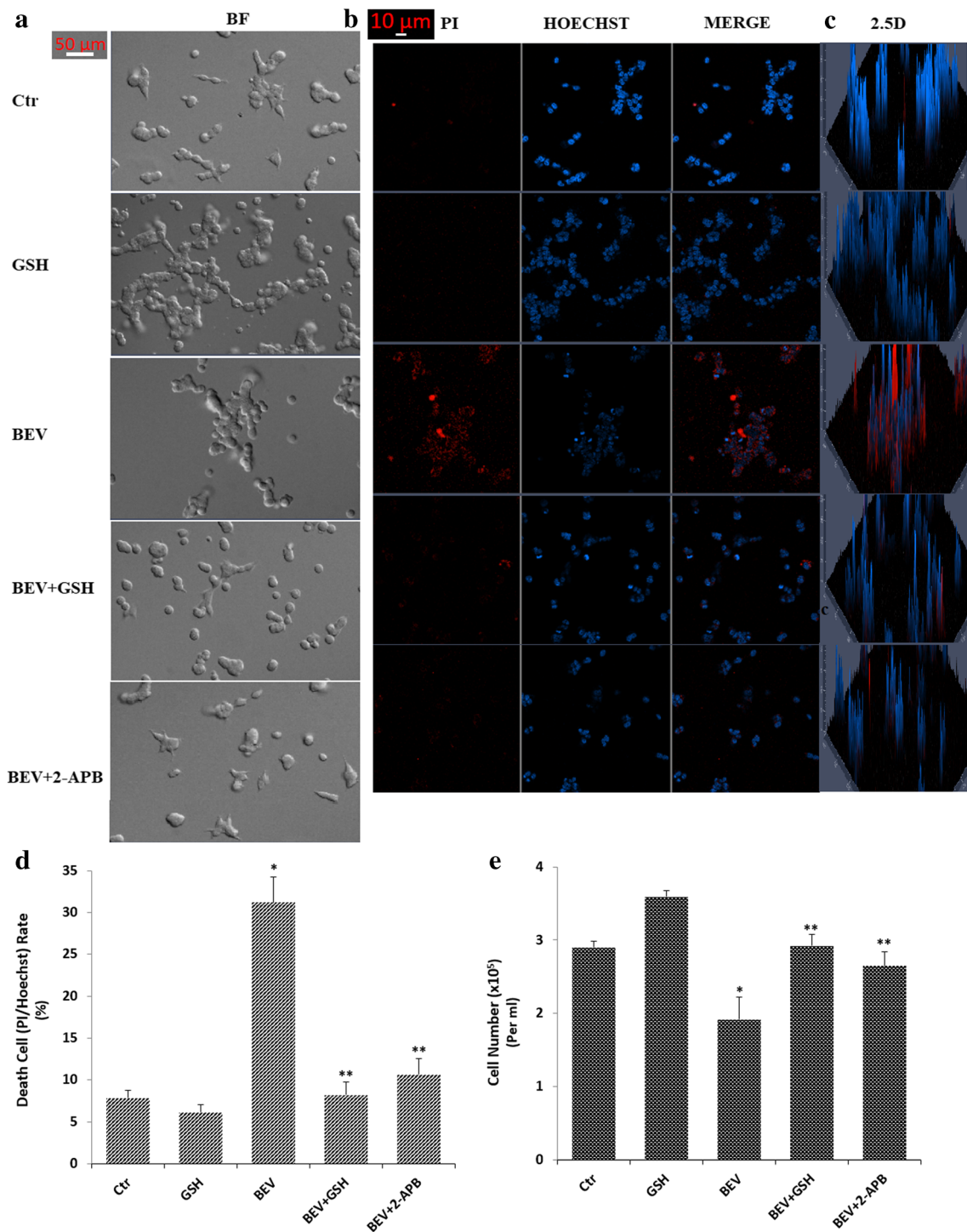


**Fig. 5** BEV-induced ARPE-19 cell death was decreased by the treatments of GSH and 2-APB, although cell number was increased by the treatments (Mean ± SD and *n* = 25–30). Representative images of bright field (BF) (a) (scale bar 50 μM), dead (propidium iodide, PI-red), and live (Hoechst 33342-blue) cell staining (scale bar 20 μM) (b), and 2.5D (c) in

the ARPE-19 cells under control or after exposure to BEV (0.25 mg/ml), GSH (10 mM), and 2-APB (0.1 mM) conditions. Fig. 5d, e. The mean percentage of PI/Hoechst rates and cell numbers, respectively. a.u. arbitrary unit. Objective 20× (\**p* ≤ 0.05 vs control (Ctr) and GSH groups. \*\**p* ≤ 0.05 vs BEV group)

modulated via inhibition of TRPM2 in the BEV-treated ARPE-19 cells by the treatment of GSH via.

An increase of Mit-Dep was predominantly induced from accumulation of excessive Ca<sup>2+</sup> into mitochondria, which

directly affects the cell survival pathways [49, 50]. Interestingly, the increase of Mit-Dep could lead to rapid activations of caspase-3 and -9 in the ARPE-19 cells [4, 19, 36]. GSH may have an antiapoptotic function interfering with Bax



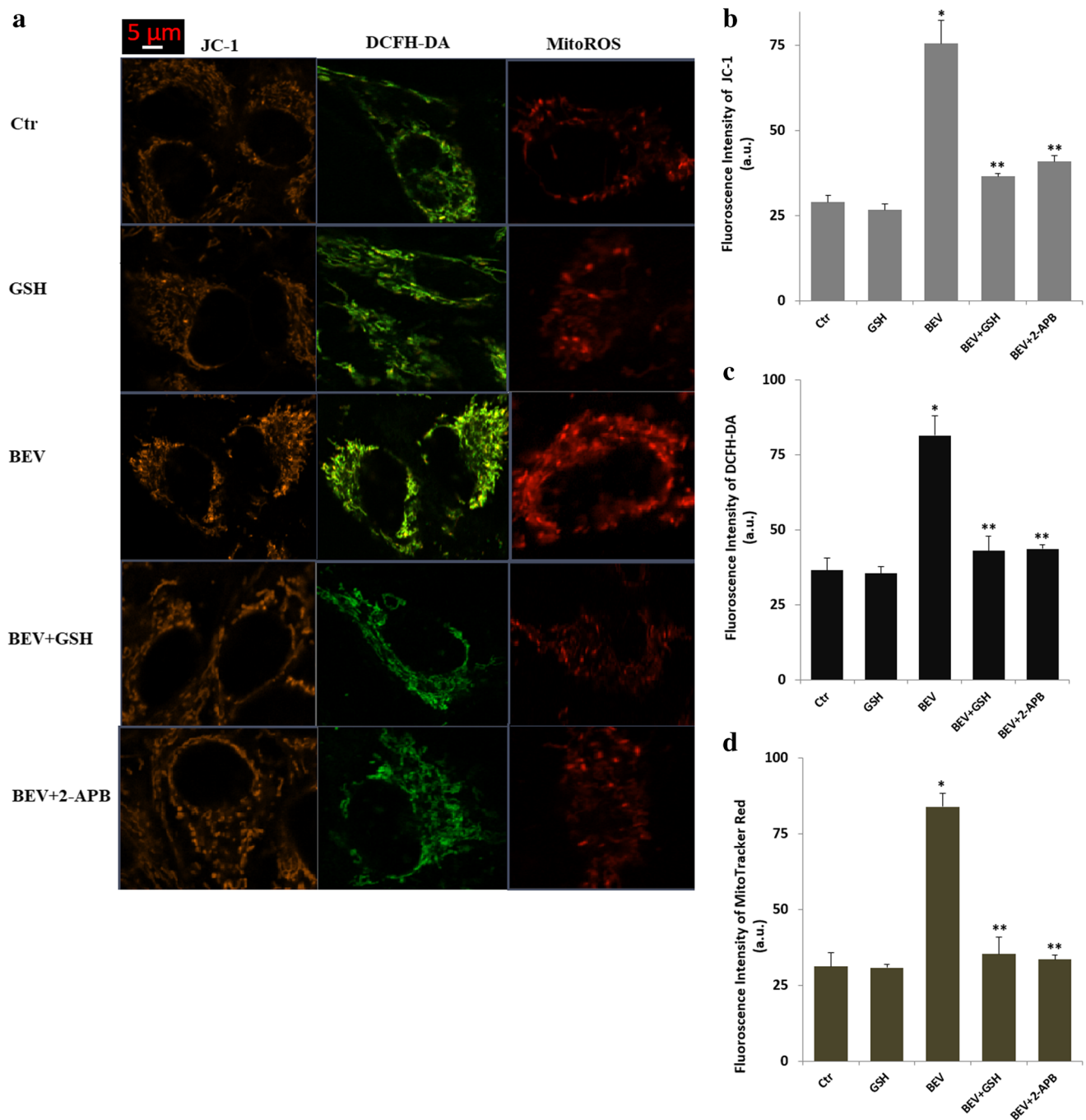


**Fig. 6** The GSH and ACA treatments reduced BEV-induced increases of Mit-Dep (JC-1), cytosolic ROS (DCFH-DA), and mitochondrial ROS (MitoROS) generations in the ARPE-19 cells (Mean  $\pm$  SD and  $n = 25$ – $30$ ). The control (Ctrl) and treatment groups (GSH (10 mM for 2 h), BEV (0.25 mg/ml for 24 h), and BEV+GSH) in the cells were induced. In the BEV+2-APB group, the cells were further incubated with 2-APB (100  $\mu$ M for 5 min) after the BEV treatment. The cells were stained with 2  $\mu$ M JC-1, 1  $\mu$ M DCFH-DA, and 1  $\mu$ M MitoTracker Red CM-H2ros

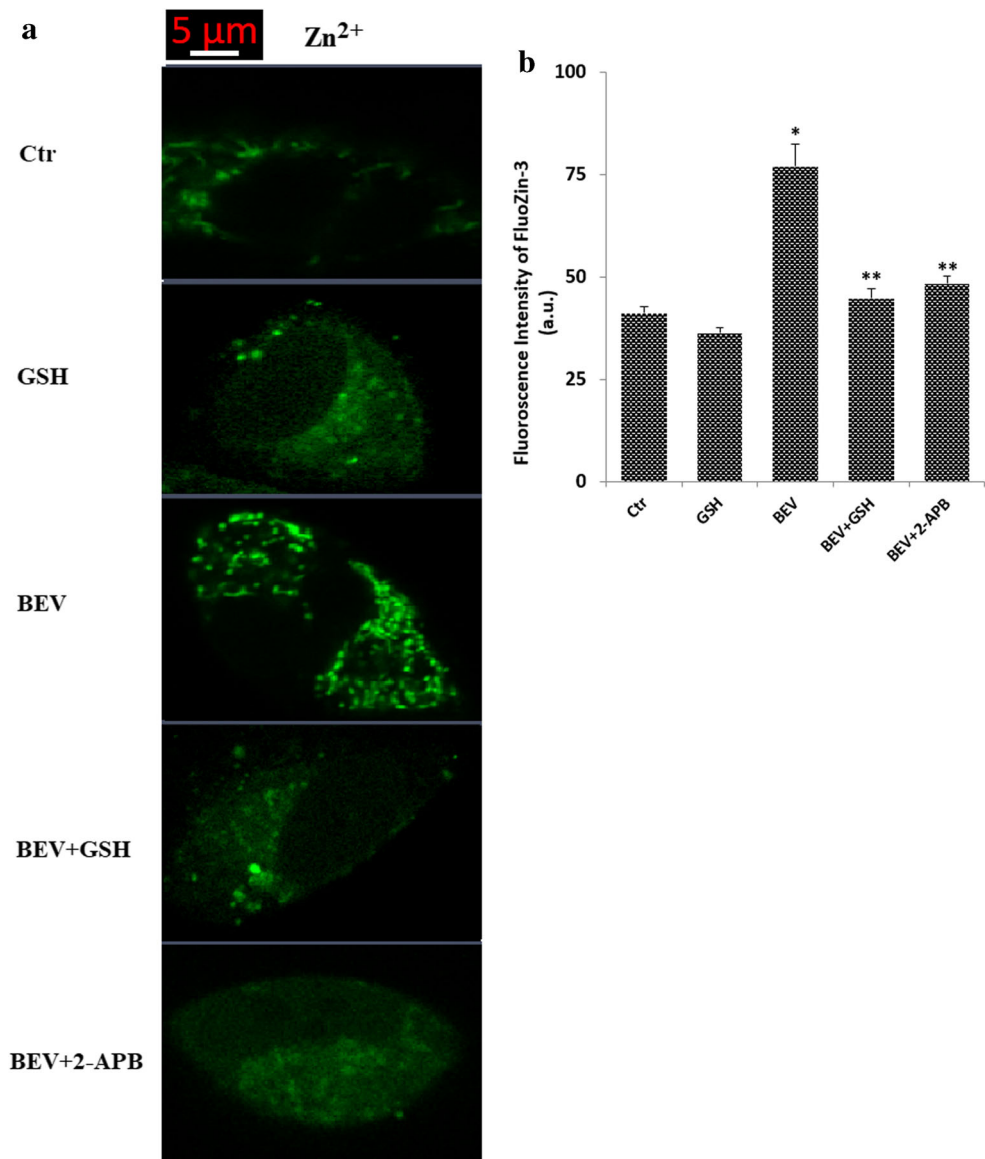
probes for measurements of Mit-Dep, cytosolic ROS, and MitoROS, respectively. The images of JC-1, DCFH-DA, and MitoROS were captured in the LSM 800 confocal microscope fitted with the  $40 \times 1.3$  oil objective. **a** The mean fluorescence intensities of the JC-1, DCFH-DA, and MitoROS were analyzed by using the ZEN software. The mean results of JC-1 (**b**), DCFH-DA (**c**), and MitoROS (**d**) were indicated as arbitrary unit (a.u.) by the columns (\* $p \leq 0.05$  vs control (Ctrl) and GSH groups. \*\* $p \leq 0.05$  vs BEV group)

proapoptotic activity [51] which consequently would be linked to the inhibition of the caspase pathway. Moreover, GSH was recently reported to upregulate GPx activity and to cause a decrease of Mit-Dep, caspase-3, and -9, which

implicates the antiapoptotic function of GSH [20]. Thus, the accumulating evidence suggests that GSH could be a survival factor directly or indirectly associated with the apoptotic pathway. Actually, GSH effectively rescued ARPE-19 cells from



**Fig. 7** The BEV-induced increase of cytosolic-free  $Zn^{2+}$  (FluoZin3) concentrations was decreased in the ARPE-19 cells by the treatment of GSH (Mean  $\pm$  SD and  $n = 25$ –30). The control (Ctr) and treatment groups, GSH (10 mM for 2 h), BEV (0.25 mg/ml for 24 h), and BEV+GSH in the ARPE-19 cells, were induced. The cells were stained with 1  $\mu$ M FluoZin3 for measurement of  $[Zn^{2+}]_c$ . The mean fluorescence intensities of FluoZin3 in the LSM 800 confocal microscope fitted with the  $40 \times 1.3$  oil objective were measured by using the ZEN software (a). The mean results of FluoZin3 fluorescence intensity were presented as arbitrary unit (a.u.) by the columns (b) (\* $p \leq 0.05$  vs control (Ctr) and GSH groups. \*\* $p \leq 0.05$  vs BEV group)



BEV-induced cell death. BEV strongly enhanced cytosolic ROS, mitochondrial ROS, caspase-3, and -9 levels via activation of TRPM2 in ARPE-19 cells that was inhibited by GSH and TRPM2 blocker (ACA and 2-APB) treatments. GSH also effectively reduced BEV-induced apoptotic cell death in the ARPE-19, as deterring cells alive by blocking apoptotic pathways. The present data confirm previous results which showed that intravitreal BEV in rabbit eyes induces mitochondrial swelling in photoreceptor inner segments and retinal expression of apoptosis (Bax, caspase-3, and -9) [52]. The increase of apoptosis as PI/annexin V rate and caspase-3 mRNA levels in the ARPE-19 [53] and human Müller cells [9] by BEV treatment under the oxidative stress ( $H_2O_2$ ) conditions was recently reported. The protective effects of antioxidants such as resveratrol and curcumin against BEV-induced adverse effects via inhibition of ROS were more recently

reported in the ARPE-19 cells [37, 48]. Contrary, it was reported that a single intravitreal injection of BEV did not result in the increase of apoptosis, caspase-3, and -9 in the porcine retina [54].

As co-factors of several antioxidant enzymes, the  $Zn^{2+}$  induced ROS scavenger and antiapoptotic actions in several cells, including ARPE-19 [55]. However, accumulation of free  $[Zn^{2+}]_c$  in mitochondria induces cell death and it is presumed to occur predominantly through mitochondrial-mediated apoptosis due to the activation of mitochondrial ROS. The mitochondrial apoptotic pathway via activations of inactive caspase-3 and -9 is induced in several cells by the increase of  $[Zn^{2+}]_c$  [35, 56]. Hence, intracellular free  $Zn^{2+}$  homeostasis is crucial for the physiological functions of ARPE-19 cells, because free  $Zn^{2+}$  can injure the ARPE-19 cells through the activation of mitochondrial-mediated

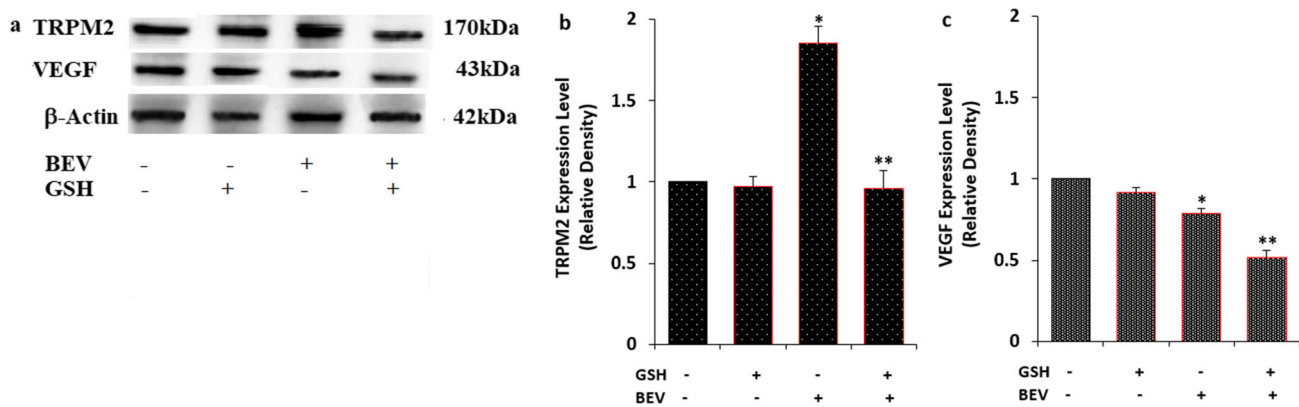


**Fig. 8** BEV-induced increases of TRPM2 channel and VEGF expressions in the ARPE-19 cells were modulated by the GSH treatment (mean  $\pm$  SD and  $n = 3$ ). The TRPM2 and VEGF expression levels were analyzed by standard Western blot analyses. For the equal protein loading,  $\beta$ -actin protein bands were used as control. Imaging,

antibody, and antigen details of the Western blot analyses were given in the material and method section. **a** Western blot bands of TRPM2, VEGF, and  $\beta$ -actin protein. **b, c** Mean values of TRPM2 and VEGF protein levels, respectively (\* $p \leq 0.05$  vs control (Ctr) and GSH groups. \*\* $p \leq 0.05$  vs BEV group)

caspace and ROS generations [57]. Hence, apoptosis, TRPM2 activation, MitoROS, and Mit-Dep levels in several cells were decreased by the depletion of  $[Zn^{2+}]_c$  [35, 58]. It was reported that accumulation of  $[Zn^{2+}]_c$  in mitochondria results in ROS generation and TRPM2 activation in neuronal cells [35, 58]. However,  $[Zn^{2+}]_c$ -induced ROS generation was decreased in neuronal cells by the GSH treatment [35, 59]. In the ARPE-19 cells, we observed that BEV caused an increase of  $[Zn^{2+}]_c$  which is associated with an increase in  $[Ca^{2+}]_c$  and ROS. We observed that the BEV-induced  $[Zn^{2+}]_c$  increase in the ARPE-19 cells was diminished by the GSH treatment.

In summary, GSH protects human ARPE-19 from BEV-induced cell death, which is closely related to the inhibition of TRPM2 activation-induced mitochondrial ROS generation and to the suppression of caspase-3 and -9 activities. This oxidant and apoptotic properties of BEV were induced through the inhibition of overload  $Ca^{2+}$  entry involving the TRPM2 activation molecular pathways. Based on this available data, we suggest that GSH via inhibition of TRPM2 may protect the ARPE-19 cells from BEV-induced mitochondrial oxidative stress and ARPE-19 cell death. Therefore, the GSH as a TRPM2 blocker may play a special role in responding to the antioxidant redox system of ARPE-19 cells and may be considered as a therapeutic approach to BEV-induced human retinal pigment epithelial cell injury.

**Authors' contributions** All authors contributed to the study conception and design. The analyses were performed by Prof. Dr. Mustafa Nazırođlu. Data analysis was performed by Assist. Prof. Dr. Dilek Özkaya. The draft of the manuscript was prepared Professor Mustafa Nazırođlu. All authors performed revision on draft of the manuscript. All authors read and approved the final manuscript.

**Funding** The current study was carried out with financial support from BSN Health, Analyses, Innovation, Consultancy, Organization, Agriculture, Industry Ltd. Inc. (Göller Bölgesi Teknokenti, Isparta, Turkey) (Project No: 2019-03. Project owner: Dr. Dilek Özkaya).

**Data availability** Present methods in the current study were induced in accordance with the relevant guidelines and regulations of BSN Health, Analyses, Innovation, Consultancy, Organization, Agriculture and Industry Ltd. (Isparta, Turkey) by including a statement in the method sections to this action. The dataset and analyses were generated in the company (BSN Health) and they are available from the corresponding author on reasonable request.

## Compliance with ethical standards

**Conflict of interest** The authors declare that they have no conflict of interest.

**Ethical approval** This article does not contain any studies with human participants or animals performed by any of the authors.

**Consent for publication** No photographs of persons were submitted.

**Code availability** Not applicable.

## References

- Shen Y, Xie C, Gu Y, Li X, Tong J (2016) Illumination from light-emitting diodes (LEDs) disrupts pathological cytokines expression and activates relevant signal pathways in primary human retinal pigment epithelial cells. *Exp Eye Res.* 145:456–467. <https://doi.org/10.1016/j.exer.2015.09.016>
- Wu HB, Yang S, Weng HY et al (2017) (2017). Autophagy-induced KDR/VEGFR-2 activation promotes the formation of vasculogenic mimicry by glioma stem cells. *Autophagy.* 13(9): 1528–1542. <https://doi.org/10.1080/15548627.2017.1336277>
- Rodríguez ML, Pérez S, Mena-Mollá S, Desco MC, Ortega ÁL (2019) Oxidative stress and microvascular alterations in diabetic retinopathy: future therapies. *Oxid Med Cell Longev.* 2019: 4940825. <https://doi.org/10.1155/2019/4940825>
- Bardak H, Uđuz AC, Bardak Y (2017) Curcumin regulates intracellular calcium release and inhibits oxidative stress parameters, VEGF, and caspase-3/-9 levels in human retinal pigment epithelium cells. *Physiol Int.* 104(4):301–315. <https://doi.org/10.1556/2060.104.2017.4.3>

5. Sreekumar PG, Kannan R, de Silva AT, Burton R, Ryan SJ, Hinton DR (2006) Thiol regulation of vascular endothelial growth factor-A and its receptors in human retinal pigment epithelial cells. *Biochem Biophys Res Commun* 346:1200–1206
6. Özkaya D, Nazıroğlu M, Armağan A, Demirel A, Köroğlu BK, Çolakoğlu N, Kükner A, Sönmez TT (2011) Dietary vitamin C and E modulates oxidative stress induced-kidney and lens injury in diabetic aged male rats through modulating glucose homeostasis and antioxidant systems. *Cell Biochem Funct.* 29(4):287–293. <https://doi.org/10.1002/cbf.1749>
7. Marazita MC, Dugour A, Marquioni-Ramella MD, Figueroa JM, Suburo AM (2016) Oxidative stress-induced premature senescence dysregulates VEGF and CFH expression in retinal pigment epithelial cells: implications for age-related macular degeneration. *Redox Biol.* 7:78–87. <https://doi.org/10.1016/j.redox.2015.11.011>
8. Byeon SH, Lee SC, Choi SH et al (2010) Vascular endothelial growth factor as an autocrine survival factor for retinal pigment epithelial cells under oxidative stress via the VEGF-R2/PI3K/Akt. *Invest Ophthalmol Vis Sci.* 51(2):1190–1197. <https://doi.org/10.1167/iovs.09.4144>
9. Matsuda M, Krempel PG, Marquezini MV et al (2017) Cellular stress response in human Müller cells (MIO-M1) after bevacizumab treatment. *Exp Eye Res.* 160:1–10. <https://doi.org/10.1016/j.exer.2017.04.005>
10. Russo V, Barone A, Conte E, Prascina F, Stella A, Noci ND (2009) Bevacizumab compared with macular laser grid photocoagulation for cystoid macular edema in branch retinal vein occlusion. *Retina.* 29(4):511–515. <https://doi.org/10.1097/IAE.0b013e318195ca65>
11. Pham B, Thomas SM, Lillie E et al (2019) Anti-vascular endothelial growth factor treatment for retinal conditions: a systematic review and meta-analysis. *BMJ Open.* 9(5):e022031. <https://doi.org/10.1136/bmjopen-2018-022031>
12. Şahiner M, Bahar D, Öner A et al (2018) The effects of anti-vascular endothelial growth factor drugs on retinal pigment epithelial cell culture. *Turk J Ophthalmol.* 48(4):190–195. <https://doi.org/10.4274/tjo.20270>
13. de Oliveira Dias JR, Rodrigues EB, Maia M, Magalhães O Jr, Penha FM, Farah ME (2011) (2011) Cytokines in neovascular age-related macular degeneration: fundamentals of targeted combination therapy. *Br J Ophthalmol.* 95(12):1631–1637. <https://doi.org/10.1136/bjo.2010.186361>
14. Fack F, Espedal H, Keunen O et al (2015) Bevacizumab treatment induces metabolic adaptation toward anaerobic metabolism in glioblastomas. *Acta Neuropathol.* 129(1):115–131. <https://doi.org/10.1007/s00401-014-1352-5>
15. Sharma RK, Rogojina AT, Chalam KV (2010) Bevacizumab therapy normalizes the pathological intraocular environment beyond neutralizing VEGF. *Mol Vis.* 16:2175–2184
16. Elgouhary SM, Elmazar HF, Naguib MI, Bayomy NR. (2020) Role of oxidative stress and vascular endothelial growth factor expression in pterygium pathogenesis and prevention of pterygium recurrence after surgical excision [published online ahead of print, 2020 Jun 6]. *Int Ophthalmol.* <https://doi.org/10.1007/s10792-020-01440-2>.
17. Miura Y, Klettner A, Roider J (2010) VEGF antagonists decrease barrier function of retinal pigment epithelium in vitro: possible participation of intracellular glutathione. *Invest Ophthalmol Vis Sci.* 51(9):4848–4855
18. Brar VS, Sharma RK, Murthy RK, Chalam KV (2010) Bevacizumab neutralizes the protective effect of vascular endothelial growth factor on retinal ganglion cells. *Mol Vis.* 16:1848–1853
19. Yazıcı T, Koçer G, Nazıroğlu M, Övey İS, Öz A (2018) Zoledronic acid, bevacizumab and dexamethasone-induced apoptosis, mitochondrial oxidative stress, and calcium signaling are decreased in human osteoblast-like cell line by selenium treatment. *Biol Trace Elem Res.* 184(2):358–368. <https://doi.org/10.1007/s12011-017-1187-8>
20. Nazıroğlu M (2007) New molecular mechanisms on the activation of TRPM2 channels by oxidative stress and ADP-ribose. *Neurochem Res.* 32(11):1990–2001
21. Nazıroğlu M, Lückhoff A (2008) Effects of antioxidants on calcium influx through TRPM2 channels in transfected cells activated by hydrogen peroxide. *J Neurol Sci.* 270(1-2):152–158. <https://doi.org/10.1016/j.jns.2008.03.003>
22. Hara Y, Wakamori M, Ishii M, Maeno E, Nishida M, Yoshida T et al (2002) LTRPC2 Ca<sup>2+</sup>-permeable channel activated by changes in redox status confers susceptibility to cell death. *Mol Cell.* 9(1):163–173. [https://doi.org/10.1016/S1097-2765\(01\)00438-5](https://doi.org/10.1016/S1097-2765(01)00438-5)
23. Övey İS, Nazıroğlu M (2015) Homocysteine and cytosolic GSH depletion induce apoptosis and oxidative toxicity through cytosolic calcium overload in the hippocampus of aged mice: involvement of TRPM2 and TRPV1 channels. *Neuroscience* 284:225–233. <https://doi.org/10.1016/j.neuroscience.2014.09.078>
24. Belrose JC, Xie YF, Gierszewski LJ, MacDonald JF, Jackson MF (2012) Loss of glutathione homeostasis associated with neuronal senescence facilitates TRPM2 channel activation in cultured hippocampal pyramidal neurons. *Mol Brain.* 5:11. <https://doi.org/10.1186/1756-6606-5-11>
25. Özgül C, Nazıroğlu M (2012) TRPM2 channel protective properties of N-acetylcysteine on cytosolic glutathione depletion dependent oxidative stress and Ca<sup>2+</sup> influx in rat dorsal root ganglion. *Physiol Behav.* 106(2):122–128. <https://doi.org/10.1016/j.physbeh.2012.01.014>
26. Nazıroğlu M, Özgül C, Çiğ B, Doğan S, Uğuz AC (2011) Glutathione modulates Ca<sup>2+</sup> influx and oxidative toxicity through TRPM2 channel in rat dorsal root ganglion neurons. *J Membr Biol.* 242(3):109–118. <https://doi.org/10.1007/s00232-011-9382-6>
27. Lee M, Cho T, Jantaratnotai N, Wang YT, McGeer E, McGeer PL (2010) Depletion of GSH in glial cells induces neurotoxicity: relevance to aging and degenerative neurological diseases. *FASEB J.* 24(7):2533–2545. <https://doi.org/10.1096/fj.09-149997>
28. Yıldızhan K, Nazıroğlu M (2020) Glutathione depletion and parkinsonian neurotoxin MPP<sup>+</sup>-induced TRPM2 channel activation play central roles in oxidative cytotoxicity and inflammation in Microglia. *Mol Neurobiol.* 57(8):3508–3525. <https://doi.org/10.1007/s12035-020-01974-7>
29. Nazıroğlu M, Lückhoff A. (2008) Effects of antioxidants on calcium influx through TRPM2 channels in transfected cells activated by hydrogen peroxide. *J Neurol Sci.* 15, 270(1-2):152-158. <https://doi.org/10.1016/j.jns.2008.03.003>.
30. Duzgun Ergun D, Dursun S, Pastaci Ozsobaci N, Hatırnaz Ng O, Nazıroğlu M, Ozcelik D (2020 Apr) (2020) The potential protective roles of zinc, selenium and glutathione on hypoxia-induced TRPM2 channel activation in transfected HEK293 cells. *J Recept Signal Transduct Res.* 30:1–10. <https://doi.org/10.1080/10799893.2020.1759093>
31. Meléndez García R, Arredondo Zamarripa D, Arnold E et al (2016) Prolactin protects retinal pigment epithelium by inhibiting sirtuin 2-dependent cell death. *EBioMedicine.* 7:35–49. <https://doi.org/10.1016/j.ebiom.2016.03.048>
32. Mittal M, Urao N, Hecquet CM et al (2015) Novel role of reactive oxygen species-activated Trp melastatin channel-2 in mediating angiogenesis and posts ischemic neovascularization. *Arterioscler Thromb Vasc Biol.* 35(4):877–887. <https://doi.org/10.1161/ATVBAHA.114.304802>
33. Dunn KC, Aotaki-Keen AE, Putkey FR, Hjelmeland LM (1996) ARPE-19, a human retinal pigment epithelial cell line with differentiated properties. *Exp Eye Res.* 62(2):155–169. <https://doi.org/10.1006/exer.1996.0020>



34. Sun Y, Sukumaran P, Selvaraj S et al (2018) TRPM2 Promotes neurotoxin MPP<sup>+</sup>/MPTP-induced cell death. *Mol Neurobiol*. 55(1):409–420. <https://doi.org/10.1007/s12035-016-0338-9>
35. Akyuva Y, Nazıroğlu M (2020) Resveratrol attenuates hypoxia-induced neuronal cell death, inflammation and mitochondrial oxidative stress by modulation of TRPM2 channel. *Sci Rep*. 10(1):6449. <https://doi.org/10.1038/s41598-020-63577-5>
36. Argun M, Tök L, Uğuz AC, Çelik Ö, Tök ÖY, Nazıroğlu M (2014) Melatonin and amfenac modulate calcium entry, apoptosis, and oxidative stress in ARPE-19 cell culture exposed to blue light irradiation (405 nm). *Eye (Lond)*. 28(6):752–760. <https://doi.org/10.1038/eye.2014.50>
37. Subramani M, Ponnalagu M, Krishna L, Jeyabalan N, Chevour P, Sharma A, Jayadev C, Shetty R, Begum N, Archunan G, Das D (2017) Resveratrol reverses the adverse of bevacizumab on cultured ARPE-19 cells. *Sci Rep*. 7(1):12242
38. Sedlak J, Lindsay RHC (1968) Estimation of total, protein bound and non-protein sulfhydryl groups in tissue with Ellmann's reagent. *Anal Biochem*. 25:192–205
39. Lawrence RA, Burk RF (2012) Glutathione peroxidase activity in selenium-deficient rat liver. *Biochem Biophys Res Commun*. 425(3):503–509
40. Placer ZA, Cushman L, Johnson BC (1966) Estimation of products of lipid peroxidation (malonyl dialdehyde) in biological fluids. *Anal Biochem*. 16:359–364
41. Erel O (2004) A novel automated direct measurement method for total antioxidant capacity using a new generation, more stable ABTS radical cation. *Clinical Biochemistry* 37:277–285
42. McHugh D, Flemming R, Xu SZ, Perraud AL, Beech DJ (2003) Critical intracellular Ca<sup>2+</sup> dependence of transient receptor potential melastatin 2 (TRPM2) cation channel activation. *J Biol Chem*. 278(13):11002–11006. <https://doi.org/10.1074/jbc.M210810200>
43. Latzer P, Shchyglo O, Hartl T, Matschke V, Schlegel U, Manahan-Vaughan D, Theiss C. (2019) Blocking VEGF by bevacizumab compromises electrophysiological and morphological properties of hippocampal neurons. *Front Cell Neurosci*. 26:13:113. <https://doi.org/10.3389/fncel.2019.00113>.
44. Han D, Wu X, Liu L, Shu W, Huang Z. (2018) Sodium tanshinone IIA sulfonate protects ARPE-19 cells against oxidative stress by inhibiting autophagy and apoptosis. *Sci Rep*. 2018;8(1):15137. <https://doi.org/10.1038/s41598-018-33552-2>.
45. Dilsiz N, Olcucu A, Cay M, Nazıroğlu M, Cobanoglu D (1999) Protective effects of selenium, vitamin C and vitamin E against oxidative stress of cigarette smoke in rats. *Cell Biochem Funct*. 17(1):1–7. [https://doi.org/10.1002/\(SICI\)1099-0844\(199903\)17:1](https://doi.org/10.1002/(SICI)1099-0844(199903)17:1)
46. Li X, Zhang M, Zhou H (2014) The morphological features and mitochondrial oxidative stress mechanism of the retinal neurons apoptosis in early diabetic rats. *J Diabetes Res* 2014:678123. <https://doi.org/10.1155/2014/678123>
47. Sabet NS, Atashbar S, Khanlou EM, Kahrizi F, Salimi A (2020) Curcumin attenuates bevacizumab-induced toxicity via suppressing oxidative stress and preventing mitochondrial dysfunction in heart mitochondria. *Naunyn Schmiedebergs Arch Pharmacol*. 393(8):1447–1457. <https://doi.org/10.1007/s00210-020-01853-x>
48. Nanegrungsunk D, Apaijai N, Yarana C, Sripetchwandee J, Limpastan K, Watcharasaksilp W, Vaniyapong T, Chattipakorn N, Chattipakorn SC (2016) Bevacizumab is superior to Temozolomide in causing mitochondrial dysfunction in human brain tumors. *Neurol Res*. 38(4):285–293. <https://doi.org/10.1080/01616412.2015.1114233>
49. Carrasco C, Rodríguez BA, Pariente JA (2015) Melatonin as a stabilizer of mitochondrial function: Role in diseases and aging. *Turk J Biol*. 39:822–831
50. Uğuz AC, Cig B, Espino J, Bejarano I, Nazıroğlu M, Rodríguez AB, Pariente JA (2012) (2012) Melatonin potentiates chemotherapy-induced cytotoxicity and apoptosis in rat pancreatic tumor cells. *J Pineal Res*. 53(1):91–98
51. Habermann KJ, Grünwald L, van Wijk S, Fulda S (2017) Targeting redox homeostasis in rhabdomyosarcoma cells: GSH-depleting agents enhance auranofin-induced cell death. *Cell Death Dis*. 8(10):e3067. <https://doi.org/10.1038/cddis.2017.412>
52. Inan UU, Avci B, Kusbeci T, Kaderli B, Avci R, Temel SG (2007) Preclinical safety evaluation of intravitreal injection of full-length humanized vascular endothelial growth factor antibody in rabbit eyes. *Invest Ophthalmol Vis Sci* 48:1773–1781
53. Kim S, Kim YJ, Kim NR, Chin HS (2015) Effects of bevacizumab on Bcl-2 expression and apoptosis in retinal pigment epithelial cells under oxidative stress. *Korean J Ophthalmol*. 29(6):424–432. <https://doi.org/10.3341/kjo.2015.29.6.424>
54. Iandiev I, Francke M, Makarov F, Hollborn M, Uhlmann S, Wurm A et al (2011) Effects of intravitreal bevacizumab (Avastin) on the porcine retina. *Graefes Arch Clin Exp Ophthalmol*. 249(12):1821–1819. <https://doi.org/10.1007/s00417-011-1773-y>
55. Maret W (2019) The redox biology of redox-inert zinc ions. *Free Radic Biol Med*. 134:311–326. <https://doi.org/10.1016/j.freeradbiomed.2019.01.006>
56. Hashemi M, Ghavami S, Eshraghi M, Booy EP, Los M (2007) Cytotoxic effects of intra and extracellular zinc chelation on human breast cancer cells. *Eur J Pharmacol*. 14:557(1):9-19. <https://doi.org/10.1016/j.ejphar.2006.11.010>
57. Song J, Lee SC, Kim SS, Koh HJ, Kwon OW, Kang JJ, Kim EK, Shin SH, Lee JH (2004) Zn<sup>2+</sup>-induced cell death is mediated by the induction of intracellular ROS in ARPE-19 cells. *Curr Eye Res*. 28(3):195–201. <https://doi.org/10.1076/ceyr.28.3.195.26251>
58. Mortadza SS, Sim JA, Stacey M, Jiang LH (2017) Signalling mechanisms mediating Zn(2+)-induced TRPM2 channel activation and cell death in microglial cells. *Sci Rep*. 7:45032. <https://doi.org/10.1038/srep45032>
59. Zhou ZD, Lim TM (2010) Glutathione conjugates with dopamine-derived quinones to form reactive or non-reactive glutathione-conjugates. *Neurochem Res*. 35(11):1805–1818. <https://doi.org/10.1007/s11064-010-0247-7>

**Publisher's note** Springer Nature remains neutral with regard to jurisdictional claims in published maps and institutional affiliations.